UNIVERSITY OF AMSTERDAM

UvA-DARE (Digital Academic Repository)

New eruptive variable(s) in the RAFGL7009S HII region

Nikoghosyan, E.H.; Azatyan, N.M.; Andreasyan, D.H.; Kaper, L.; Yeghikyan, A.G.; Baghdasaryan, D.S.; Harutyunyan, N.A.

DOI
10.1093/mnras/stad1111

Publication date
2023

Document Version
Final published version

Published in
Monthly Notices of the Royal Astronomical Society

Link to publication

Citation for published version (APA):
Nikoghosyan, E. H., Azatyan, N. M., Andreasyan, D. H., Kaper, L., Yeghikyan, A. G., Baghdasaryan, D. S., & Harutyunyan, N. A. (2023). New eruptive variable(s) in the RAFGL 7009S HII region. *Monthly Notices of the Royal Astronomical Society*, *522*(2), 2171-2180. https://doi.org/10.1093/mnras/stad1111

General rights
It is not permitted to download or to forward/distribute the text or part of it without the consent of the author(s) and/or copyright holder(s), other than for strictly personal, individual use, unless the work is under an open content license (like Creative Commons).

Disclaimer/Complaints regulations
If you believe that digital publication of certain material infringes any of your rights or (privacy) interests, please let the Library know, stating your reasons. In case of a legitimate complaint, the Library will make the material inaccessible and/or remove it from the website. Please Ask the Library: https://uba.uva.nl/en/contact, or a letter to: Library of the University of Amsterdam, Secretariat, Singel 425, 1012 WP Amsterdam, The Netherlands. You will be contacted as soon as possible.

UvA-DARE is a service provided by the library of the University of Amsterdam (https://dare.uva.nl)

Download date:21 Apr 2025

Monthly Notices of the ROYAL ASTRONOMICAL SOCIETY

MNRAS **522,** 2171–2180 (2023)
Advance Access publication 2023 April 14

https://doi.org/10.1093/mnras/stad1111

New eruptive variable(s) in the RAFGL 7009S H II region

E. H. Nikoghosyan,[1]★ N. M. Azatyan,[1] D. H. Andreasyan,[1] L. Kaper,[2] A. L. Samsonyan,[1] A. G. Yeghikyan,[1] D. S. Baghdasaryan[1] and N. A. Harutyunyan[3]

[1]*Byurakan Astrophysical Observatory, 0213 Aragatsotn Province, Armenia*
[2]*Anton Pannekoek Institute for Astronomy, University of Amsterdam, Science Park 904, NL-1098 XH Amsterdam, The Netherlands*
[3]*Department of Physics, Yerevan State University, 1 Alex Manoogian Street, 0025 Yerevan, Armenia*

Accepted 2023 April 13. Received 2023 April 13; in original form 2022 August 30

ABSTRACT

Eruptions of young stellar objects (YSOs) are rare events, therefore a new outburst is always noteworthy. We present two new high-amplitude variable YSOs, J183421.85−055951.0 (#1) and J183421.39−055937.7 (#2), in the RAFGL 7009S star-forming region. We find them in the United Kingdom Infrared Telescope Infrared Deep Sky Survey Galactic Plane Survey data base, and supplement these data with archived infrared and millimetre photometric and spectral images and data from the *Spitzer* Infrared Array Camera, the *K*-band Multi-Object Spectrograph, and the Atacama Large Millimeter/submillimeter Array data bases. The outburst in #1 occurred in the period 2007–2011, during which the brightness increased by ∼2.7 mag in the *K* band and by ∼2.5 mag in the 3.6 μm band. The colour indices indicate a YSO in Class I/II evolutionary stage. After outburst, the *K*-band spectrum shows the *CO* band, Brγ, Mg I in absorption and H_2 in emission – characteristics associated with a FU Orionis (FUors)-type eruptive variable. Object #1 is associated with an outflow detected in the near-infrared and millimetre ranges, mainly in the H_2, SiO, HCO+, and HCN lines. Object #2 only shows high-amplitude variability in the *K* band ($\Delta K = 2.0$ mag) while its colour indices before outburst indicate a YSO at an early evolutionary stage. There is no obvious outflow activity associated with this object. We classify #1 as a FUor-type eruptive variable based on the obtained data. The limited information on #2 makes it difficult to draw definite conclusions about the nature of its variability.

Key words: stars: individual: UKIDSS-J183421.85−055951.0, UKIDSS-J183421.39−055937.7 – stars: pre-main sequence – infrared: stars.

1 INTRODUCTION

In recent years, the events of episodic accretion in young stellar objects (YSOs) with associated eruptive variability have attracted increasing attention from observers and theorists. The reason for this attention is the accretion process, a fundamental part of the formation and evolution of stars and planets, is still poorly understood (Hartmann, Herczeg & Calvet 2016; Fischer et al. 2022). Because outbursts of YSOs are explained exactly by short lived major increases in circumstellar disc accretion (Hartmann & Kenyon 1996), the eruptive variables are of great interest given their potential importance to a wide range of star and planet formation processes. Among other issues, episodic accretion is a major unresolved matter in low-mass star formation (Audard et al. 2014) due to the effect that it may have on the masses and ages inferred from Hertzsprung–Russell (HR) diagrams for pre-main-sequence (PMS) clusters. Historically, steady accretion scenarios have been proposed to describe the PMS stage (e.g. Shu 1977; Terebey, Shu & Cassen 1984). However, for low-mass Class I YSOs, the stellar luminosity predicted by steady accretion models is an order of magnitude fainter than observed in nearby clusters (e.g. Kenyon et al. 1990; Caratti o Garatti et al. 2012). If episodic accretion is common in early stellar evolution, it could solve the so-called luminosity problem in low-mass embedded protostars (Guo et al. 2020).

Classically, the eruptive YSOs have been divided into two main subclasses: FU Orionis (FUors)- and EX Lupi (EXors)-type. FUor-type YSOs show large increases (up to 6 mag in the optical range) in flux that last for decades to centuries and recurrence of those outbursts is still unknown (Hartmann & Kenyon 1996). In contrast, EXor-type YSOs show moderate outbursts (about 2.5 – 5 mag in optical) that last for a few months to a few years and recur (Herbig 2008). Ongoing studies show that the peak brightness and the subsequent evolution of the light curve differ significantly among representatives of each class (Audard et al. 2014; Fischer et al. 2022, and references therein).

These two classes of objects also have significantly different spectral characteristics. During an outburst, FUors have typical spectral characteristics, which can be understood as a rapidly accreting disc that overshines the central protostar at all wavelengths. Some FUors have peak accretion rates in excess of $10^{-4}\,M_\odot\,yr^{-1}$, while others only reach 10^{-6}–$10^{-5}\,M_\odot\,yr^{-1}$ (Audard et al. 2014; Fischer et al. 2022, and references therein). In the optical range, FUors have absorption spectra similar to an F or G supergiant, with broad blueshifted absorption lines indicating strong winds, a P Cygni profile for the Hα line, and strong Li absorption at 6707 Å (Hartmann & Kenyon 1996). In the infrared (IR) range, spectra of FUors resemble K or M giants or supergiants, with strong CO, TiO, or VO absorption bands and, in addition to weak metal absorptions (Connelley & Reipurth 2018). The optical and near-infrared (NIR)

★ E-mail: elena@bao.sci.am

© 2023 The Author(s)
Published by Oxford University Press on behalf of Royal Astronomical Society

Downloaded from https://academic.oup.com/mnras/article/522/2/2171/7120044 by University Library, University of Amsterdam user on 11 July 2024

spectra of EXors in the quiescent stage contain metallic bands (Na, Ca, K, Fe, Ti, and Si) and in some cases the *CO* band in absorption. The stars appear to be typically young, late-type stellar photospheres. During the outburst, when the luminosity of the disc increases and it can outshine the stellar photosphere, most absorption lines turn into emission lines, and many emission lines become stronger, including the H I recombination lines (Herbig 2008; Rigliaco et al. 2020, and references therein). The peak of the accretion rate ($\dot{M}$) is of the order of a few 10^{-7} $M_\odot$ yr^{-1} during an outburst and about 10^{-10} – 10^{-9} $M_\odot$ yr^{-1} in a quiescent period (Audard et al. 2014; Fischer et al. 2022, and references therein).

Outburst types are usually classified from light curves and/or spectra, but not consistently. Many outbursting YSOs have peculiar properties and do not fit into the two classical categories in terms of their light curves or spectroscopic properties. The prototype of this type of object is the V1647 Ori eruptive variable (Briceño et al. 2004). The object is deeply embedded and most likely at an early evolutionary stage (Mosoni et al. 2013). With time, the number of objects that cannot be included in the optically defined classification has increased significantly, and Contreras Peña et al. (2017b) have suggested considering such eruptive variables as a subclass, 'MNors', given the similarity to V1647 Ori. This subclass includes a significant number of embedded Class I YSOs (Guo et al. 2021). However, at present, there is no unified physics that describes the MNors subclass (Fischer et al. 2022).

In recent years, significant progress has been made in the study of YSO eruptive variables, including an increased number of identified objects, their photometric and spectral characteristics, and their impact on mass accretion (e.g. Connelley & Reipurth 2018; Fischer et al. 2022, and references therein). The United Kingdom Infrared Telescope Infrared Deep Sky Survey Galactic Plane Survey (UKIDSS GPS) contributed significantly to this progress (Lucas et al. 2008). The survey includes several epochs of *K*-band photometry to find brief and rarely observed phases of stellar evolution via detecting high-amplitude variability, including YSO outbursts. A series of works have shown that eruptive variability is at least an order of magnitude more common in Class I YSOs than Class II YSOs (e.g. Contreras Peña et al. 2017a, b; Guo et al. 2021). Based on 1.3-mm continuum observations of 10 FUors and FUor-like objects, Kóspál et al. (2021) assumed that FUor discs are generally more massive and compact than the discs of Class I/II objects, suggesting different interpretations. In particular, whether an atypical structure of the circumstellar discs is formed during the evolution, or whether some discs are originally born with a smaller radius and a larger mass than usual?

Several scenarios have been proposed to explain the triggering of FUor outbursts: magnetorotational instability (Zhu et al. 2009) or thermal instability (Hartmann & Kenyon 1996) of the circumstellar disc, the presence of a companion in an eccentric orbit (Bonnell & Bastien 1992) or a large body (e.g. a planet or a large 'gas blob') in a circumstellar disc (e.g. Vorobyov et al. 2021), as well as a rapidly rotating bloated star near the edge of instability (Herbig, Petrov & Duemmler 2003). However, despite all efforts, there is no consensus on the cause of the outbursts. Therefore, new data related to eruptive variables are important.

This work aims to present two new high-amplitude IR variable YSOs (#1 J183421.85−055951.0 and #2 J183421.39−055937.7) found using the UKIDSS GPS data base. The objects are located in the RAFGL 7009S (G25.65+1.05, IRAS 18316−0602) active star-forming region. The location of the H_2 emission features indicates the likely presence of more than one outflow in this region (Varricatt et al. 2010). The region is maser-rich, including both Class I and II methanol, OH, and H_2O masers (e.g. Bayandina et al. 2019, and references therein). This region recently achieved notoriety due to its recurring maser burst behaviour, exhibiting kJy bursts on several occasions (Bayandina et al. 2019; Volvach et al. 2019). Zavagno et al. (2002) have suggested that the central source of RAFGL 7009S is not a single YSO but associated with a cluster of embedded massive YSOs. Moreover, using the stellar surface density distribution, Azatyan, Nikoghosyan & Khachatryan (2016) and Andreasyan et al. (2020) have shown that in the vicinity of RAFGL 7009S, there is a group of YSOs within ∼0.5′ radius, in which, based on the IR colour indices, 40 potential members with IR excess were identified.

Table 1. (J-K) colour indices and UKIDSS GPS *K*-band magnitudes of 10 supporting stars.

ID	(J-K)	*K* (2007)	*K* (2011)
J183419.62−060006.1	0.51	14.06 ± 0.01	14.06 ± 0.01
J183418.89−055952.3	0.95	14.08 ± 0.01	14.10 ± 0.01
J183421.12−055931.4	0.98	15.89 ± 0.03	15.89 ± 0.03
J183421.68−055926.6	1.03	16.58 ± 0.05	16.50 ± 0.05
J183421.75−060010.0	1.00	16.74 ± 0.06	16.70 ± 0.05
J183419.04−055951.9	0.97	14.55 ± 0.01	14.53 ± 0.01
J183422.19−060011.9	1.14	15.52 ± 0.02	15.54 ± 0.02
J183422.18−060003.2	1.21	15.90 ± 0.03	15.87 ± 0.03
J183421.31−060025.2	1.27	17.36 ± 0.11	17.36 ± 0.11
J183418.91−060007.2	1.15	16.14 ± 0.04	16.16 ± 0.04

The distance of the region is disputed. Very long baseline interferometry measurements of trigonometric parallax have never been performed in this region. Molecular line observations, in most cases, favour a close kinematic distance and yield a value of 2.7 kpc (Sunada et al. 2007). In contrast, H I self-absorption towards the source suggests a greater kinematic distance of 12.5 kpc (Green & McClure-Griffiths 2011). A probability density function for the distance to the source, calculated based on the Bar and Spiral Structure Legacy Survey (BeSSeL; Reid et al. 2016) indicates a distance of 2.08 ± 0.37 kpc with a probability of 64 per cent. In our calculations below, we will apply the latter value.

We have organized the paper as follows: Section 2 describes the data used; Section 3 describes the photometric properties (Section 3.1), evolutionary stage (Section 3.2), and spectral data (Section 3.3) of the new eruptive variables. Finally, the results are discussed and summarized in Section 4.

2 USED DATA

To identify and study eruptive variable YSOs #1 and #2, we acquired archival IR and millimetre photometric and spectroscopic data and images. For the *NIR* bands, the photometric data from DR7 and DR11 of UKIDSS GPS (Lucas et al. 2008) were employed. The survey is complete to approximately 19.0 and 18.1 mag in the *H* and *K* bands, respectively. The resolution of the images is 0.4 arcsec/pixel. For our study, we used magnitudes obtained through an aperture with a radius of 2.5 pixel or 1 arcsec(AperMag3), which are recommended for both point and extended sources (Hodgkin et al. 2009). We also acquired *K* and H_2 band images from Varricatt et al. (2010), which were obtained on the United Kingdom Infrared Telescope (UKIRT) in 2003. Photometric measurements on this *K*-band image were carried out under the standard process using the IRAF APPHOT package and an aperture with a radius of 1 arcsec. The magnitudes of 10 supporting stars were used to calibrate the flux (see Table 1). The NIR colour index of these stars corresponds to the MS objects.

Downloaded from https://academic.oup.com/mnras/article/522/2/2171/7120044 by University Library, University of Amsterdam user on 11 July 2024

In addition, they have practically the same *K*-band magnitudes in the UKIDSS GPS surveys at different epochs of observation and a 90 per cent probability ('Merged source class' is −1) of being point sources. From the average magnitudes of these stars, the zero-point magnitude was determined to be 21.43 ± 0.05 mag.

For the mid-infrared (MIR) bands, we acquired *Spitzer* Infrared Array Camera 3.6 and 4.5 μm band images and data (Fazio et al. 2004) from the *Spitzer* Science Archive. These include the data obtained by SIRTF GPS (2006), GLIMPSE 3D (2008), and Deep GLIMPSE (2012, 2014, and 2016) programmes. For photometric measurements, the zero-point fluxes of the 3.6 and 4.5 μm bands (Vega-standard magnitudes for 1 DN s^{-1}) were adopted from Reach et al. (2005). An aperture radius of 4 pixels (∼ 3.5 arcsec) was used with an adjoining sky annulus width of 1 pixel.

The *K*-band spectral observations were carried out on 2014 July 15 with the *K*-band Multi-Object Spectrograph (KMOS; Project ID: 093.C-0669; PI: Suzanne Ramsay; Target: IRAS 18316−0602), and they are publicly available from the European Southern Observatory (ESO) archive. KMOS is a multi-object NIR spectrograph with a spectral resolution of R ∼ 4200 (Sharples et al. 2014), mounted in the Nasmyth focus of the ESO Very Large Telescope (VLT). The display and analysis of the KMOS spectra were performed using the Spectral Analysis Tool for the Virtual Observatory (SPLAT VO) graphical tool (Castro-Neves & Draper 2014). The equivalent width (EW) was estimated by summing $(1 - F_i/C_i)$ over the wavelength range, where F_i and C_i are the flux and the estimated continuum level at the pixel *i*, respectively. For photometric measurements, we computed the integrated intensity (Moment 0) map in the *K* band using channels where the emission differed from zero. The flux is referenced to the Vega magnitude system (https://www.eso.org/observing/etc/doc/infoetc.html) and *K* magnitudes obtained through aperture equal to 1 arcsec .

We also used the observations of the Atacama Large Millimeter/submillimeter Array (ALMA) Three-millimetre Observations of Massive Star-forming regions (ATOMS) project (Liu et al. 2020). The ATOMS survey was conducted with the Atacama Compact 7-m Array (ACA; Morita Array) and the 12-m array with band 3 (Project ID: 2019.1.00685.S; PI: Tie Liu). This paper used observations from the 12-m array, available on the ALMA archive. The observations were performed on 2019 October 31. The angular resolution and maximum recovering angular scale for the 12-m array observations are ∼1.2–1.9 arcsec and ∼14.5–20.3 arcsec, respectively. Complete information about this ATOMS observation is available in Liu et al. (2020). We used three spectral windows with a bandwidth of 58.59 MHz to cover lines such as SiO (2-1), HCO+(1-0), and HCN (1-0) with rest frequencies of 86.846 96, 89.188 526, and 88.631 847 GHz, respectively. These lines are good tracers of dense gas, hot cores, shocks, infall, and outflow (Liu et al. 2017). Imaging was performed using the CASA software package, version 6.4 (McMullin et al. 2007).

3 RESULTS

3.1 Photometric variability

A comparison of the NIR and MIR images in the vicinity of the RAFGL 7009S H II region revealed two stellar objects with significant brightness variability named as #1 and #2. Neither object has been identified as a variable in previous studies, including the UKIDSS GPS survey (Lucas et al. 2017). Their images and photometric data at different epochs and wavelengths are shown in Fig. 1 and Tables 2 and 3. The photometric data in the tables were taken from Zavagno et al. (2002; obtained from UKIRT) and data bases or determined from the NIR and MIR images for this study.

Both variable stellar objects were practically indetectable in DENIS K_S, and 2MASS J, H, and K_S images. Most likely, the brightness of the stellar objects in 1999 was so low ($K_S > 15.0$ mag) that the sensitivity and resolution of these surveys do not allow their identification (Epchtein et al. 1999; Skrutskie et al. 2006). The spatial resolutions of the *Spitzer* Multiband Imaging Photometer (MIPS), the Wide-field Infrared Survey Explorer (WISE), AKARI, and other longer wavelength surveys in this H II region with significant surface brightness and stellar density do not allow the variable stellar objects to be resolved. In addition, the RAFGL 7009S region is associated with a powerful water maser (Bayandina et al. 2019; Burns et al. 2020), whose variability may be accompanied by flux variability in the IR and sub-mm bands (Gray et al. 2020, and references therein). Therefore, changes in the emission intensity in the same ranges obtained at different epochs are likely the result of the maser outbursts. The stellar variability effect on the total flux in longer wavelengths could be insignificant.

Fig. 2 shows the light curves of both variables plotted from the photometric data in Tables 2 and 3. In 1996 and 2003, the brightness of #1 in the *K* band was low. Then, in the period from 2003 to 2007, the brightness increased only slightly ($\Delta K = \sim$0.3 mag); however, in the period from 2007 to 2011, #1 brightened significantly, by almost 2.7 mag. Such difference in brightness is commensurate with or even exceeds the ΔK of some embedded eruptive variables in Contreras Peña et al. (2017b). According to the MIR data, a significant increase in brightness in the 3.6 μm band (∼2.5 mag) occurred during the period 2006–2012, remaining at the same level in 2014 and 2015 in both the 3.6- and 4.5-μm bands. Based on these data, #1 erupted during the period 2007–2011.

The light curve of #2 is more complicated than the light curve of #1. In 1996, the object was 0.5 mag brighter in the *K* band than in 2003 and 2007. Then, between 2007 and 2011, as in the previous case, the brightness in the *K* band increased significantly ($\Delta K = \sim$2.0 mag). However, in the 3.6 μm band between 2006 and 2012, the brightness decreased slightly by ∼0.5 mag. The proximity of the bright H II region made it impossible to resolve the object and determine its magnitude in the 4.5 μm band. Unfortunately, the paucity of available photometric data does not permit a more accurate recovery of the light curve.

It is not always easy to disentangle the signs of variable accretion from those of other effects, such as changing extinction, even with multiwavelength observations. Therefore, the photometric parameters of four additional stellar objects were used for comparison purposes: J183421.66−055936.4 (#3), J183421.90−055940.3 (#4), J183422.96−055953.9 (#5), and J183423.08−055950.1 (#6). Images and photometric data at different epochs and wavelengths are also shown in Fig. 1 and Tables 2 and 3. In the NIR and MIR, three of these objects (#4, #5, and #6) show almost no brightness variability within the error bars. However, #3 shows a brightness variability of an order of 0.5 mag in the 3.6 μm band.

3.2 Evolutionary stage

The IR colour indices of both the variables and other stellar objects in Tables 2 and 3 suggest that they are YSOs. The paucity of photometric data makes it impossible to construct the spectral energy distribution. However, colour–colour (cc) and colour–magnitude (cm) diagrams can be used to classify the evolutionary stage of stellar objects. The diagrams were chosen based on the available photometric data.

Downloaded from https://academic.oup.com/mnras/article/522/2/2171/7120044 by University Library, University of Amsterdam user on 11 July 2024

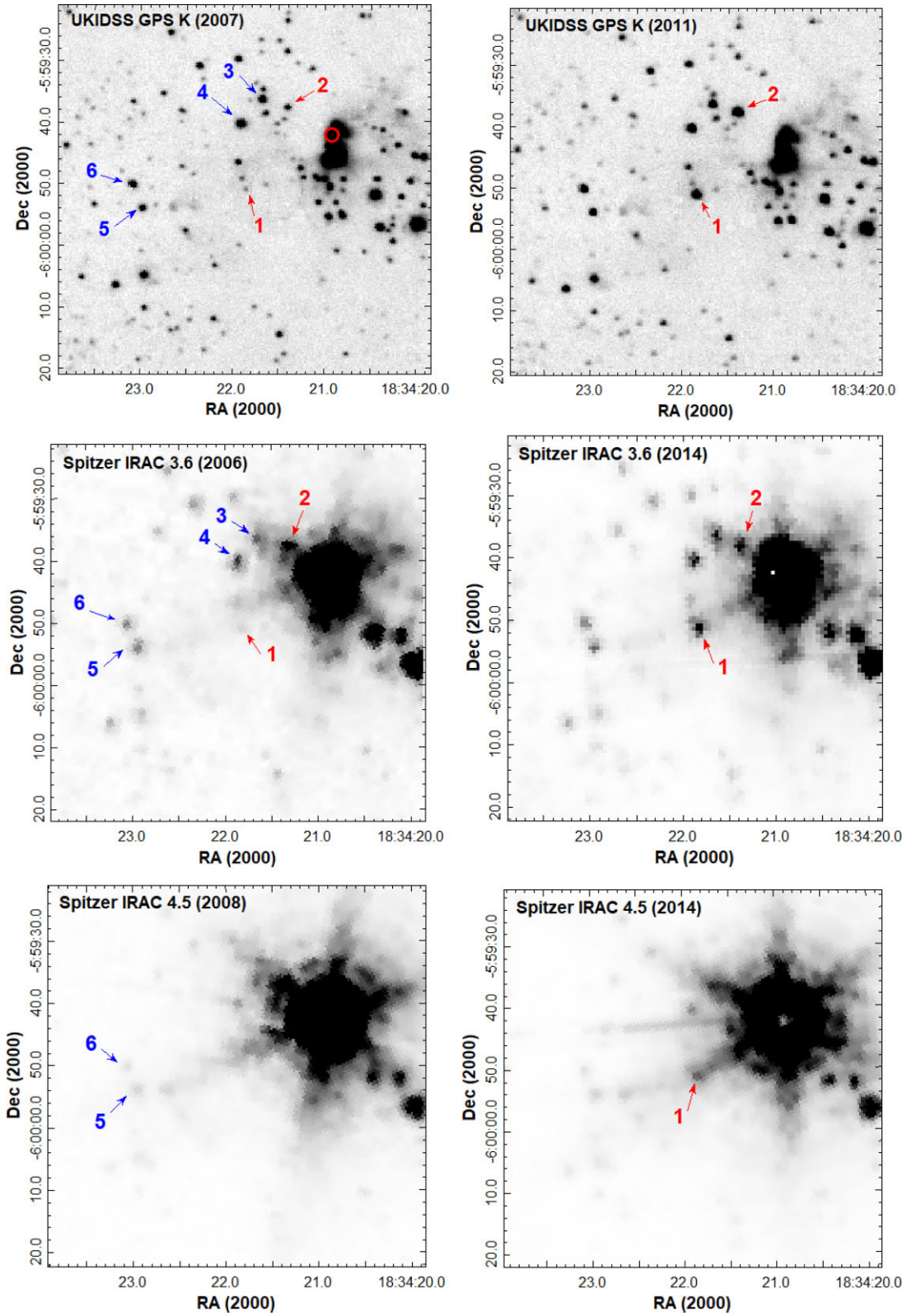

Figure 1. Images of RAFGL 7009S H II region obtained at different epochs and wavelengths. The positions of stellar objects from Tables 2 and 3 are marked. The position of IRAS 18316−0602 is marked with a red circle.

UKIDSS-J183421.85−055951.0 (#1): Allen et al. (2007) demonstrated that it is reasonably efficient to separate protostars (Class I), stars with discs (Class II), and disc-less photospheres using the K-[3.6] versus [3.6]-[4.5] cc diagram (see Fig. 3, left-hand panel), where the [3.6]-[4.5] colour is dominated by an accretion disc and not sensitive to interstellar extinction. The diagram shows the object position before and after the correction for interstellar extinction (A_V) according to Flaherty et al. (2007) correlations. On COBE/DIRBE

Downloaded from https://academic.oup.com/mnras/article/522/2/2171/7120044 by University Library, University of Amsterdam user on 11 July 2024

Table 2. NIR photometric data (*H* and *K* bands).

Object	Zavagno et al. (2002) 1996 July		Varricatt et al. (2010) 2003 June 16	UKIDSS GPS 2007 Aug 27		UKIDSS GPS 2011 Sept 18	KMOS 2014 July 15
	H	*K*	*K*	*H*	*K*	*K*	*K*
#1 J183421.85−055951.0	–	16.94	16.87 ± 0.09[a]	–	16.29 ± 0.04	13.63 ± 0.04	13.92 ± 0.10
#2 J183421.39−055937.7	17.88	14.40	14.95 ± 0.08[a]	18.50 ± 0.12	15.04 ± 0.01	13.11 ± 0.01	–
#3 J183421.66−055936.4	15.84	14.26	14.23 ± 0.08[a]	15.92 ± 0.01	14.07 ± 0.01	13.96 ± 0.01	–
#4 J183421.90−055940.3	16.39	13.73	13.59 ± 0.05[a]	15.95 ± 0.01	13.46 ± 0.01	13.45 ± 0.01	–
#5 J183422.96−055953.9	–	–	14.53 ± 0.08[a]	18.46 ± 0.11	14.59 ± 0.01	14.52 ± 0.01	14.62 ± 0.14
#6 J183423.08−055950.1	–	–	13.96 ± 0.06[a]	16.08 ± 0.01	14.13 ± 0.01	14.14 ± 0.01	14.07 ± 0.10

[a]The magnitudes in Tables 2 and 3 were measured in this study.

Table 3. MIR photometric data (3.6 and 4.5 μm bands).

Object	SIRTF GPS 2006 Sept 7	GLIMPSE 3D 2008 July 6	Deep GLIMPSE 2012 Nov 14	Deep GLIMPSE 2014 May 28		Deep GLIMPSE 2015 Jan 13
	3.6	4.5	3.6	3.6	4.5	4.5
#1 J183421.85−055951.0	14.50 ± 0.22[a]	–	11.75 ± 0.11[a]	11.98 ± 0.09[a]	11.16 ± 0.06[a]	11.20 ± 0.10[a]
#2 J183421.309−055937.7	11.66 ± 0.13[a]	–	12.11 ± 0.12[a]	12.01 ± 0.09[a]	–	–
#3 J183421.66−055936.4	12.71 ± 0.19	–	12.16 ± 0.12[a]	12.05 ± 0.17[a]	–	–
#4 J183421.90−055940.3	12.15 ± 0.10	–	12.29 ± 0.15[a]	12.23 ± 0.16	–	–
#5 J183422.96−055953.9	12.80 ± 0.06	12.19 ± 0.16	12.73 ± 0.10[a]	12.78 ± 0.07	12.31 ± 0.11	12.45 ± 0.07[a]
#6 J183423.08−055950.1	13.02 ± 0.06	12.84 ± 0.22	12.94 ± 0.11[a]	12.94 ± 0.04	12.82 ± 0.07	12.89 ± 0.07[a]

[a]The magnitudes in Tables 2 and 3 were measured in this study.

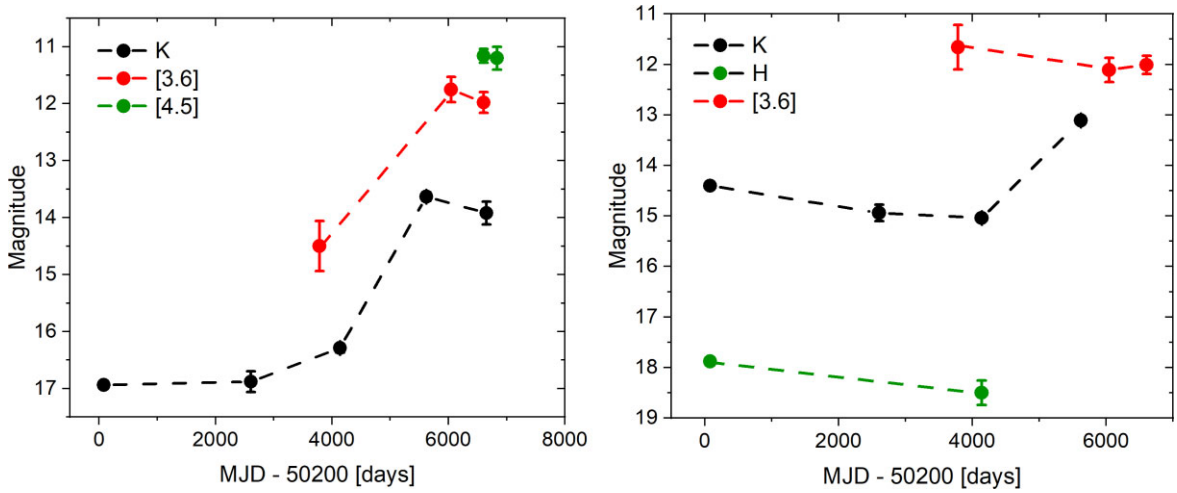

Figure 2. Light curves of #1 (*left-hand panel*) and #2 (*right-hand panel*).

and IRAS/ISSA maps (Schlegel, Finkbeiner & Davis 1998) at the object location, the A_V value is ∼8.8 mag. We used the NIR and MIR photometric data at the maximum brightness after 2011. For comparison, we also marked the positions of several eruptive variables after outbursting with Class I and II evolutionary stages obtained from Audard et al. (2014), Contreras Peña et al. (2014), Gramajo, Rodón & Gómez (2014), Nikoghosyan, Azatyan & Khachatryan (2017), and Contreras Peña et al. (2017b), and references therein. These include RNO 1B and 1C (Class II), V1057 Cyg (Class I), as well as deeply embedded OO Ser, AR 6B, UKIDSS-J185318.36+012454.5, GPS v3, and VVV v721. In this diagram, #1 occupies the intermediate position between RNO 1B and 1C and the deeply embedded YSOs at an earlier evolutionary stage. Moreover, after the extinction correction, the object shifts to the border of the Class I and II domains.

The stellar object occupies the same position on the $(K_{abs})_0$ versus $(K\text{-}[4.5])_0$ cm diagram (see Fig. 3, right-hand panel). The $(K_{abs})_0$ value was determined for a distance of 2.08 kpc (see Introduction). The Class I, II, and III domains were taken from Koenig et al. (2008). Based on the position in both diagrams and relative to other YSOs, object #1 is probably in an intermediate Class I/II evolutionary stage.

According to their position on both diagrams, #5 and #6 can be considered as YSOs at the Class II evolutionary stage. As mentioned in the introduction, previous studies have shown a young star cluster in the vicinity of the RAFGL 7009S H II region. Since the colour indices of these objects correspond to a YSO, it can be assumed that, like #1, they also belong to the cluster.

UKIDSS-J183421.39−055937.7 (#2): Due to the discrepancy between the outburst epoch in the NIR and the MIR light curve, we cannot compare the photometric data in these ranges. Therefore,

Downloaded from https://academic.oup.com/mnras/article/522/2/2171/7120044 by University Library, University of Amsterdam user on 11 July 2024

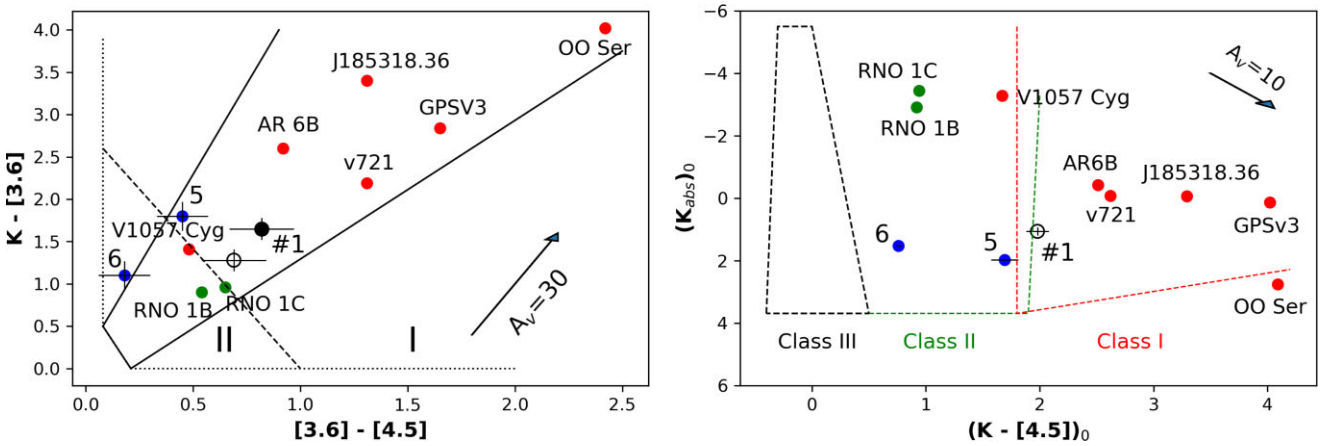

Figure 3. *Left*: *K*-[3.6] versus [3.6]-[4.5] cc diagram. The Class I and II domains are separated by the dashed line (Allen et al. 2007). Positions of #1 before and after the extinction correction are marked by filled and open black circles, respectively; #5 and #6 stellar objects – by blue circles; eruptive variables with Class II evolutionary stage (Gramajo et al. 2014) – by green circles; eruptive variables with Class I evolutionary stage (Gramajo et al. 2014) and IR eruptive variables from Contreras Peña et al. (2014, 2017b) and Nikoghosyan et al. (2017) – by red circles. *Right*: $(K_{abs})_0$ versus $(K\text{-}[4.5])_0$ cm diagram. The Class I, II, and III domains were taken from Koenig et al. (2008). The arrows show the extinction vectors (Flaherty et al. 2007).

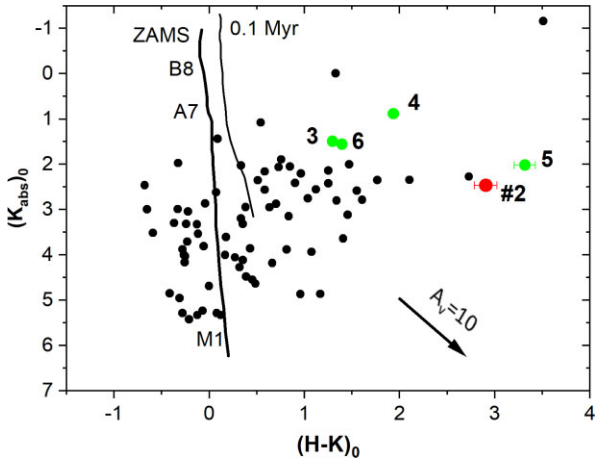

Figure 4. $(K_{abs})_0$ versus $(H–K)_0$ cm diagram. The PMS isochrones for 0.1 Myr (Siess et al. 2000) and zero-age main sequence are drawn as thin and thick solid lines, respectively. The positions of a few spectral types are labelled. The red circle marks the position of #2; green circles – #3 –#6 in Tables 2 and 3; and black circles – the point sources identified in the UKIDSS GPS-DR7 survey in 0.5 arcmin radius around IRAS 18316−0602. The arrow shows the extinction vector (Rieke & Lebofsky 1985).

to determine the evolutionary stage of this variable, the $(K_{abs})_0$ versus $(H–K)_0$ diagram was used (see Fig. 4). The PMS isochrone for 0.1 Myr was obtained from Siess, Dufour & Forestini (2000). As in the previous case, the $(K_{abs})_0$ values of the objects were determined for a distance of 2.08 kpc. The position of #2 on the diagram corresponds to the photometric data from 2007, i.e. before the outburst. This variable, as well as #3–#6, is significantly shifted to the right of the 0.1 Myr isochrone. In addition, the diagram shows the position of point sources taken from GPS UKIDSS-DR6 catalogue in 0.5 arcmin radius around IRAS 18316−0602, Taking into account the *K*-band limit of the UKIDSS survey (Lucas et al. 2008), only objects with $K < 18.02$ mag were selected. A certain number of them, including #2–#6, are shifted to the right of the isochrone, and their IR excess cannot be explained by interstellar extinction alone. This again confirms the presence of a young stellar cluster, to which, apparently, #1–#6 also belong.

3.3 Spectroscopic data

3.3.1 KMOS K-band spectral data

The *K*-band spectrum of #1 obtained in 2014 (after the outburst), is presented in Fig. 5, and Table 4 shows the EWs and the radial velocities (RVs) obtained for the atomic and molecular lines. Based on the photometric data (see Table 2 and Fig. 2), the stellar object was at maximum brightness at the epoch of the spectral observations. We found that this variable exhibits some typical characteristics of FUors outbursts (e.g. Contreras Peña et al. 2017a; Connelley & Reipurth 2018). These include strong CO absorption bands, starting at 2.29 μm. The absorption bands appear stronger than expected from the photosphere of M dwarfs and more consistent with the photospheres of late M-type supergiant and giant stars (Rayner, Cushing & Vacca 2009). The absorption of the *CO* band has previously been used as a spectroscopic signature to identify candidate FUors whose eruptions were not observed (so-called FUors-like objects, Reipurth & Aspin 2010). The authors regard this as the defining spectroscopic characteristic for these objects, given the inferred origin in a disc with a high accretion rate.

The break in the continuum at 2.29 μm due to the onset of water vapour absorption, as well as the Na I (2.21 μm) and Ca I (2.26 μm) lines are not detected above 3σ. We identified Brγ absorption and H_2 emission lines, which are frequently observed in the spectra of young stars. The H_2 emission line is usually associated with outflow activity. Among the metallic lines, only Mg I is defined. As a rule, FUors tend to have few, if any, emission lines.

Using the KMOS cube observations, we built an integrated intensity map (Moment 0) of the H_2 line (2.122 μm) and compared it with the H_2 image obtained before the outburst in 2003 (Varricatt et al. 2010). The result is shown in Fig. 6. Between these two epochs of observations, before and after the outburst, the intensity of the H_2 emission significantly increased. At the same time, the relative intensity of the neighbouring #5 and #6 objects remained almost the same. Such a significant increase in the H_2 emission could be explained by a general increase in brightness in the *K* band, but it could also be due to an increase in outflow activity during an outburst. Judging by the low EW (H_2) (−1.6 Å), it is more likely that the enhancement in flux through the H_2-band

Downloaded from https://academic.oup.com/mnras/article/522/2/2171/7120044 by University Library, University of Amsterdam user on 11 July 2024

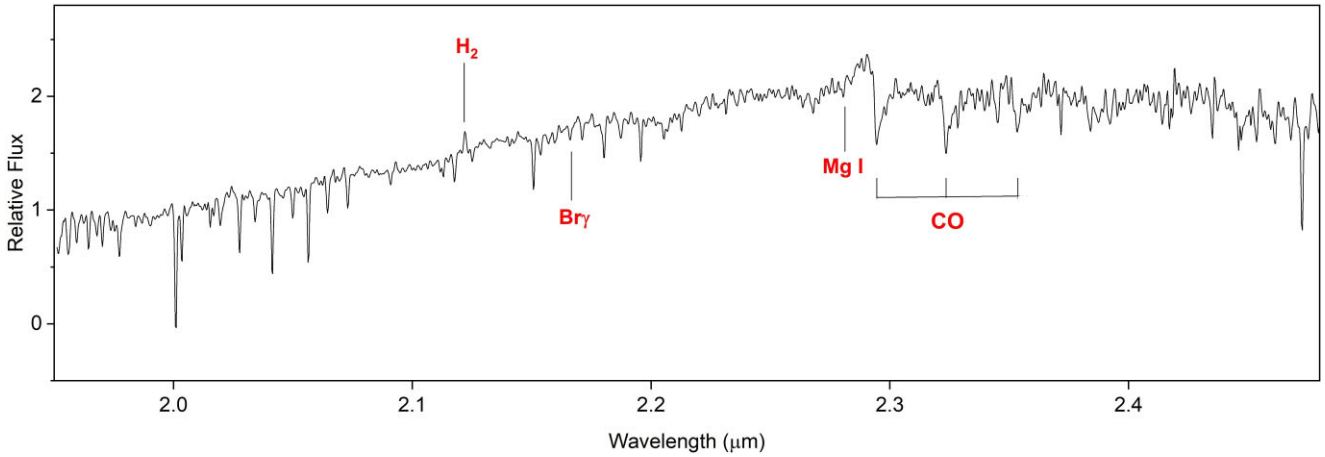

Figure 5. *K*-band spectrum of #1 obtained on 2014 July 15.

Table 4. Spectral lines of #1 in *K* band.

ID	λ (μm)	EW (Å)	RV (km s^{-1})
H_2	2.122	-1.6 ± 0.6	37.0 ± 2.7
Brγ	2.166	1.4 ± 0.9	24.2 ± 14.5
Mg I	2.280	0.7 ± 0.3	–
CO	2.293	11.7 ± 2.0	69.3 ± 16.7
CO	2.322	12.0 ± 2.5	–
CO	2.352	10.8 ± 3.0	–

Note. The EW of CO was measured by vizually selecting two continuum points around the CO bandhead and estimating the continuum as a linear function between the two points. The spectral resolution is R ∼ 4200 (Sharples et al. 2014).

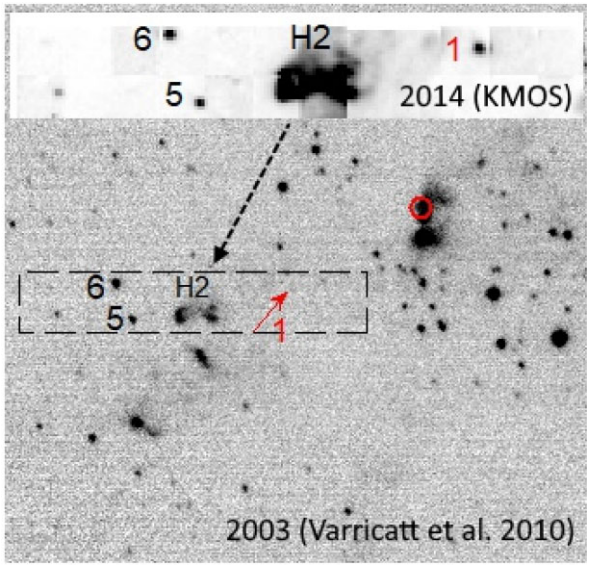

Figure 6. The H_2 $\nu = 1-0$ S(1) (2.122 μm) image (2003) taken from Varricatt et al. (2010). The inset presents the integrated intensity map (Moment 0) of the KMOS cube at the same wavelength (2014). The positions of the stellar objects from Tables 2 and 3 (#1, #5, and #6), IRAS 18316−0602 (red circle), are marked, as well as the H_2 emission feature (H2).

filter is dominated by a continuum rather than by an emission line.

Based on the spectral data, it can be concluded that #1 belongs to the FUors-type variable subclass from the presence of one of the main characteristics, specifically, the CO absorption band at maximum brightness. In addition, excluding the H_2 line, no emission lines are observed in the spectrum. However, according to the generalized data in Connelley & Reipurth (2018), the existence and the ratio of emission/absorption lines vary somewhat from object to object. For example, water absorption is not detected in several eruptive variables, including RNO 1c, BBW 76, AR 6 ab, IRAS 06393+0913, and V346 Nor. Emission lines are observed in objects such as V2494 Cyg, PP 13S, L1551 IRS5, Z CMa, and CB 230 IRS1. This list can be continued with IR eruptive variables from Contreras Peña et al. (2017b).

3.3.2 *ALMA sub-mm data*

Fig. 7 presents the blueshifted and redshifted high-velocity emission (left-hand panels), the integrated intensity (Moment 0) maps of SiO, HCO+, and HCN (middle panels) and their spectra (right-hand panels). These lines are good tracers of shock and outflow. The spectra were obtained by averaging over a 3 arcsec radius area at the position of #1 and #2. We fitted the spectra of SiO with Gaussian profiles, and the results [peak intensity, I_P, systemic velocity, V_{lsr}, and line width, full width at half-maximum (FWHM)] from Gaussian fits of the spectra for both objects are summarized in Table 5. The spectrum at the #2 position can be fitted with a single Gaussian profile (pink line), while the spectrum at the #1 position is better fitted with two Gaussians, including one narrow component (red line) and one broad component (green line). The broad component of the SiO spectrum is blueshifted by ∼6 km s^{-1} from the systemic velocity, taken from Urquhart et al. (2018; 42.8 km s^{-1}). This velocity difference indicates that #1 could be related to large-scale colliding flows that induce low-velocity shocks (Liu et al. 2020). The blueshifted emission in the SiO spectrum is consistent with the velocity of the H_2 line (2.122 μm) measured from the KMOS data.

There are certain differences between the spectral characteristics of objects #1 and #2. There are absorption features in the HCO+ and HCN spectra, which are especially well pronounced towards #2. Liu et al. (2017) have suggested that these absorption features could be caused by self-absorption or foreground clouds along the line of sight. The HCO+ and HCN emissions towards #1 show extremely high-velocity wings, indicating that outflows dominate them. No line wings in HCO+ and HCN are detected towards star #2.

Because SiO, HCO+, and HCN are good indicators of outflow, we integrated the intensity in different velocity ranges: from 0 to 38 kms^{-1} and from 45 to 75 kms^{-1} for SiO, from 15 to 38 kms^{-1} and

Downloaded from https://academic.oup.com/mnras/article/522/2/2171/7120044 by University Library, University of Amsterdam user on 11 July 2024

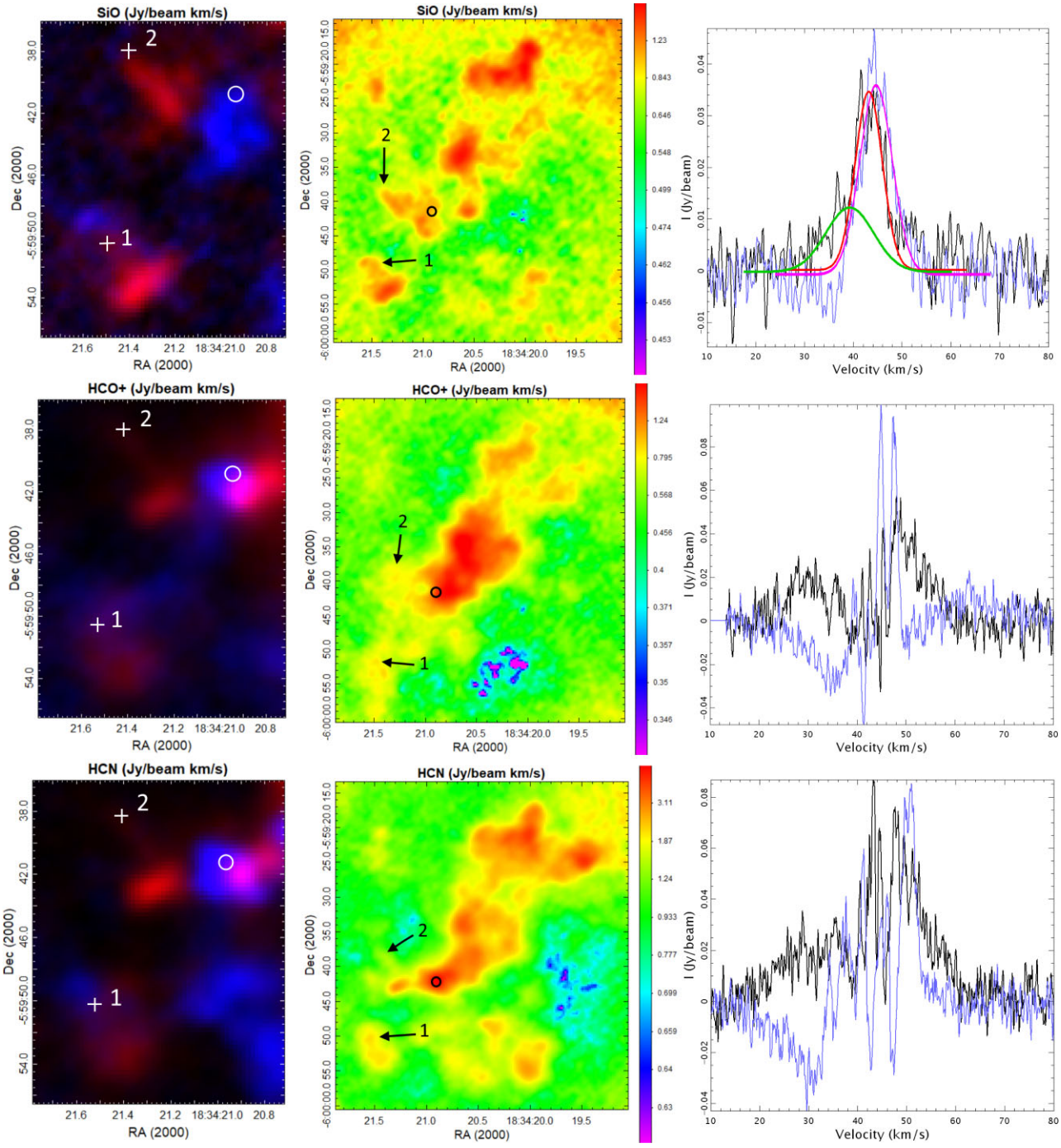

Figure 7. *Left-hand panels*: redshifted and blueshifted high-velocity emission of three lines. Object #1 and #2 are marked by crosses. *Middle panels*: the integrated intensity maps (Moment 0). Black arrows show the positions of the objects. RAFGL 7009S is marked by circles. *Right-hand panels*: spectra of Object #1 (black) and #2 (blue) stars. Green and red lines are Gaussian fitting results for #1, and the pink line is for #2.

Table 5. Parameters of SiO lines towards #1 and #2.

Objects	I_p (mJybeam^{-1})	V_{lsr} (kms^{-1})	FWHM (kms^{-1})
#1	15	36.9	10.9
–	34	43.5	5.40
#2	34	44.7	6.51

from 43 to 69 kms^{-1} for HCO+, and from 12 to 37 kms^{-1} and from 50 to 76 kms^{-1} for HCN. The colour-composite maps are presented in Fig. 7 (left-hand panel), where blueshifted high-velocity components are shown in blue and redshifted ones in red. There are pronounced blue and red lobes close to object #1, especially in the SiO map. This arrangement of lobes indicates a bipolar outflow associated with this variable. Presumably, the outflow has a large inclination angle relative to the line of sight. Varricatt et al. (2010) have assumed the presence of more than one outflow in the RAFGL 7009S H II region.

Downloaded from https://academic.oup.com/mnras/article/522/2/2171/7120044 by University Library, University of Amsterdam user on 11 July 2024

Several sources of H_2 are located close to this variable and can be the NIR tracers of outflow.

The redshifted and blueshifted emissions are not distinguishable around #2. This cannot be taken as proof of the absence of outflow. The outflow lobes of this variable star may be overlapped along the line of sight. But in this case, the spectral lines should have broad blue and redshifted wings that we do not detect. In all cases, there is no obvious evidence of an outflow associated with it.

4 DISCUSSION AND CONCLUSION

The analysis of archival data has revealed two new high-amplitude variable stellar objects, #1 (UKIDSS-J183421.85−055951.0) and #2 (UKIDSS-J183421.39−055937.7) in the RAFGL 7009S star-forming region.

UKIDSS-J183421.85−055951.0 (#1): According to the UKIDSS GPS data base, from 2007–2011, the brightness of this object in the *K* band increased by almost 2.7 mag and remained at the same high level until 2014. A significant increase in brightness (∼2.5 mag) was also found in the MIR (3.6 μm band) in the period from 2006 to 2012, remaining at the same level in 2015 in the 4.5 μm band. The colour indices indicate that it is a YSO at Class I/II evolutionary stage, which suggests that this stellar object belongs to a young cluster associated with the RAFGL 7009S H II region (Azatyan et al. 2016).

Numerous studies have shown that the accretion rate can vary significantly during the formation of YSOs. This, in turn, leads to long-term high-amplitude brightness variability in optical and NIR ranges, including bursts (Δm = ∼1 – 2.5 mag and duration from ∼1 week to 1 yr) and outbursts (Δm = ∼2.5 – 6.0 mag and duration of many years), which are mainly observed near the end stages of the main stellar accretion phase (Fischer et al. 2022, and references therein). However, changes in extinction along the line of sight also can produce larger changes in the magnitude on longer time-scales (e.g. Bouvier et al. 2013). In this case however the amplitude of the variability in brightness would be different in the NIR and MIR ranges. In addition, the brightness variability of two neighbouring stellar objects (#5 and #6 in Tables 2 and 3) is insignificant, but they also have a significant IR excess and probably belong to the same young star cluster. Therefore, based on the light curves in the NIR and MIR ranges (long duration and almost the same high amplitude of the outburst), it can be concluded that the increase in brightness of #1 have an eruptive nature. This is consistent with the findings in Scholz, Froebrich & Wood (2013) and Hillenbrand & Rodriguez (2022), who report that the threshold of brightness change to identify candidate FUor outbursts is typically about 1 – 2 mag in MIR. In the case of Object #1, the increase in brightness in the 3.6 μm band is higher. Based on the epochs of photometric data, it can be assumed that a powerful outburst in #1 occurred in the period 2007–2011.

Numerous studies suggest that FUors in outburst have several common spectroscopic characteristics that are widely interpreted as forming in a self-luminous accretion disc (Fischer et al. 2022, and references therein). According to Connelley & Reipurth (2018), during the outburst, in the IR a strong absorption in the *CO* bands, starting at 2.29 μm, is one of the most prominent spectroscopic characteristics in the NIR for FUor-type eruptive variables. In addition, FUors tend to have only a few, if any, emission lines. The existence and ratio of emission/absorption lines vary somewhat from object to object. In the KMOS *K*-band spectrum of object #1 obtained after the outburst in 2014, when the brightness of the object remained at the same high level, the *CO* absorption band is pronounced. In addition, Brγ and Mg I were found in absorption, and only H_2 was observed in emission. In general, the spectrum of this variable corresponds to the main characteristics of FUors.

We compared the properties of #1 with three embedded IRS YSOs (VVVv322, VVVv717, and VVVv721), which have been classified as eruptive variables (Contreras Peña et al. 2017b; Guo et al. 2020). The outburst amplitudes in the *K* band of the first two are commensurate with our object (ΔK = 2.63 and 2.47 mag), but in the third, it is noticeably smaller (ΔK = 1.86 mag). However, in the *MIR* band, the outburst amplitude of all three variables is noticeably smaller (Δ[3.6] = 1.8 mag, ΔW1 = 1.1 and 1.5 mag). All eruptive variables, including #1, show a CO 2.29 μm absorption, which appears stronger than expected from a stellar photosphere, with a lack of Na I and Ca I. Otherwise, there are some differences: H_2O absorption bands are observed only in VVVv322 and VVVv721; H_2 2.12 μm emission (as in #1) is seen only in VVVv322 and VVVv717. Nevertheless, all of these objects are spectroscopically similar to FUors; however, only VVVv721 shows a light curve that could place it in the FUor subclass. The other two objects (VVVv322 and VVVv717) show significant fluctuations in brightness (up to 2 mag) and are classified as MNors. The light curves of #1 and VVVv721 are almost the same. The combination of NIR and MIR photometric data shows that after the outburst between 2011 and 2015, the brightness of #1 remained at the same high level with small fluctuations. Thus, we classify this YSO as a FUor-type variable.

Another argument in favour of including #1 in the FUor subclass is the detection of a wide-angle outflow in the millimetre range, mainly in the SiO, HCO+, and HCN lines. The presence of an outflow is also demonstrated by H_2 emission in the *K*-band spectrum. The outflow itself cannot be considered direct evidence. Outflows are also often associated with YSOs that show no signs of eruptive outbursts. However, based on ALMA observations, Hales et al. (2020) have suggested that outflow activity is more inherent in FUors than in EXors.

In conclusion, most of the mechanisms that explain eruptive variability, such as bursts due to binary interaction (Bonnell & Bastien 1992), magnetorotational instability (Zhu et al. 2009) or thermal instabilities (Hartmann & Kenyon 1996), predict outbursts during Class I through Class II stages of YSO evolution, which corresponds to the evolutionary stage of #1.

UKIDSS-J183421.39−055937.7 (#2): Due to the lack of sufficient information about this object, it is difficult to draw definite conclusions. We can only say with some certainty that this high-amplitude variable (ΔK = ∼2.0 mag) YSO was at an early evolutionary stage before the outburst, and it belongs to the young stellar cluster associated with the RAFGL 7009S H II region. The set of photometric data allows us to make two assumptions about the nature of its variability. First, it is a short-term eruptive variable with a time-scale less than 1 – 2 yr or an EXors-type variable (Herbig 2008). The lack of photometric data between the epochs of observations does not allow us to substantiate this assumption. However, it is not excluded that the brightness variability is due to a change in the extinction along the line of sight. This assumption agrees with the presence of absorption features in the HCO+ and HCN spectra. To some extent, this is supported by the fact that the neighbouring #3 also shows brightness variability but in the MIR range.

In all cases, further studies are needed both to clarify the nature of the variability of #2 and to confirm the classification of #1.

Downloaded from https://academic.oup.com/mnras/article/522/2/2171/7120044 by University Library, University of Amsterdam user on 11 July 2024

ACKNOWLEDGEMENTS

We thank the anonymous reviewer for constructive comments and suggestions. This work was made possible by a research grant number No 21AG-1C044 from Science Committee of Ministry of Education, Science, Culture and Sports of Republic of Armenia. This research has made use of the data obtained at the United Kingdom Infrared Telescope, which is supported by the National Aeronautics and Space Administration and operated under an agreement among the University of Hawaii, the University of Arizona, and Lockheed Martin Advanced Technology Center; operations are enabled through the cooperation of the East Asian Observatory. We thank our colleagues in the Galactic Legacy Infrared Mid-Plane Survey Extraordinaire and Mthe ultiband Imaging Photometer *Spitzer* Legacy Surveys. This research has made use of the services of the European Southern Observatory (ESO) Science Archive Facility. This paper has made use of the following the Atacama Large Millimeter/submillimeter Array (ALMA) data: ADS/JAO.ALMA#2019.1.00685.S. ALMA is a partnership of ESO (representing its member states), National Science Foundation (USA) and the National Institutes of Natural Sciences (Japan), together with the National Research Council of Canada, the Ministry of Science and Technology, the Academia Sinica Institute of Astronomy and Astrophysics of Taiwan, and Korea Astronomy and Space Science Institute, in cooperation with the Republic of Chile. The Joint ALMA Observatory is operated by ESO, Associated Universities/National Radio Astronomy Observatory, and the National Astronomical Observatory of Japan.

DATA AVAILABILITY

The data used in this study will be made available by the corresponding authors upon request.

REFERENCES

Allen L. et al., 2007, in Reipurth B., Jewitt D., Keil K.eds, Protostars and Planets V. University of Arizona Press, Tucson, p. 361
Andreasyan D., Azatyan N., Nikoghosyan E., Harutyunian H., Baghdasaryan D., 2020, Commun. Byurakan Astrophys. Obs., 67, 335
Audard M. et al., 2014, in Beuther H., Klessen R. S., Dullemond C. P., Henning T.eds, Protostars and Planets VI. University of Arizona Press, Tucson, p. 387
Azatyan N. M., Nikoghosyan E. H., Khachatryan K. G., 2016, Astrophysics, 59, 339
Bayandina O. S., Burns R. A., Kurtz S. E., Shakhvorostova N. N., Val'tts I. E., 2019, ApJ, 884, 140
Bonnell I., Bastien P., 1992, ApJ, 401, L31
Bouvier J., Grankin K., Ellerbroek L. E., Bouy H., Barrado D., 2013, A&A, 557, A77
Briceño C. et al., 2004, ApJ, 606, L123
Burns R. A. et al., 2020, MNRAS, 491, 4069
Caratti o Garatti A. et al., 2012, A&A, 538, A64
Castro-Neves M., Draper P. W., 2014, Astrophysics Source Code Library, record ascl:1402.008
Connelley M. S., Reipurth B., 2018, ApJ, 861, 145
Contreras Peña C. et al., 2014, MNRAS, 439, 1829
Contreras Peña C. et al., 2017a, MNRAS, 465, 3011
Contreras Peña C. et al., 2017b, MNRAS, 465, 3039
Epchtein N. et al., 1999, A&A, 349, 236
Fazio G. G. et al., 2004, ApJS, 154, 10
Fischer W. J., Hillenbrand L. A., Herczeg G. J., Johnstone D., Kóspál Á., Dunham M. M., 2022, preprint (arXiv:2203.11257)
Flaherty K. M., Pipher J. L., Megeath S. T., Winston E. M., Gutermuth R. A., Muzerolle J., Allen L. E., Fazio G. G., 2007, ApJ, 663, 1069
Gramajo L. V., Rodón J. A., Gómez M., 2014, AJ, 147, 140
Gray M. D., Etoka S., Travis A., Pimpanuwat B., 2020, MNRAS, 493, 2472
Green J. A., McClure-Griffiths N. M., 2011, MNRAS, 417, 2500
Guo Z. et al., 2020, MNRAS, 492, 294
Guo Z. et al., 2021, MNRAS, 504, 830
Hales A. S. et al., 2020, ApJ, 900, 7
Hartmann L., Kenyon S. J., 1996, ARA&A, 34, 207
Hartmann L., Herczeg G., Calvet N., 2016, ARA&A, 54, 135
Herbig G. H., 2008, AJ, 135, 637
Herbig G. H., Petrov P. P., Duemmler R., 2003, ApJ, 595, 384
Hillenbrand L. A., Rodriguez A. C., 2022, Res. Notes Am. Astron. Soc., 6, 6
Hodgkin S. T., Irwin M. J., Hewett P. C., Warren S. J., 2009, MNRAS, 394, 675
Kenyon S. J., Hartmann L. W., Strom K. M., Strom S. E., 1990, AJ, 99, 869
Koenig X. P., Allen L. E., Gutermuth R. A., Hora J. L., Brunt C. M., Muzerolle J., 2008, ApJ, 688, 1142
Kóspál Á. et al., 2021, ApJS, 256, 30
Liu T. et al., 2017, ApJ, 849, 25
Liu T. et al., 2020, MNRAS, 496, 2790
Lucas P. W. et al., 2008, MNRAS, 391, 136
Lucas P. W. et al., 2017, MNRAS, 472, 2990
McMullin J. P., Waters B., Schiebel D., Young W., Golap K., 2007, in Shaw R. A., Hill F., Bell D. J.eds, ASP Conf. Ser. Vol. 376, Astronomical Data Analysis Software and Systems XVI. Astron. Soc. Pac., San Francisco, p. 127
Mosoni L. et al., 2013, A&A, 552, A62
Nikoghosyan E. H., Azatyan N. M., Khachatryan K. G., 2017, A&A, 603, A26
Rayner J. T., Cushing M. C., Vacca W. D., 2009, ApJS, 185, 289
Reach W. T. et al., 2005, PASP, 117, 978
Reid M. J., Dame T. M., Menten K. M., Brunthaler A., 2016, ApJ, 823, 77
Reipurth B., Aspin C., 2010, in Harutyunian H. A., Mickaelian A. M., Terzian Y.eds, Evolution of Cosmic Objects through their Physical Activity, "Gitutyun" Publishing House of NAS RA, Yerevan, Armenia,p. 19
Rieke G. H., Lebofsky M. J., 1985, ApJ, 288, 618
Rigliaco E. et al., 2020, A&A, 641, A33
Schlegel D. J., Finkbeiner D. P., Davis M., 1998, ApJ, 500, 525
Scholz A., Froebrich D., Wood K., 2013, MNRAS, 430, 2910
Sharples R. et al., 2014, in Ramsay S. K., McLean I. S., Takami H.eds, Proc. SPIE Conf. Ser. Vol. 9147, Ground-Based and Airborne Instrumentation for Astronomy V. SPIE, Bellingham, p. 91470W
Shu F. H., 1977, ApJ, 214, 488
Siess L., Dufour E., Forestini M., 2000, A&A, 358, 593
Skrutskie M. F. et al., 2006, AJ, 131, 1163
Sunada K., Nakazato T., Ikeda N., Hongo S., Kitamura Y., Yang J., 2007, PASJ, 59, 1185
Terebey S., Shu F. H., Cassen P., 1984, ApJ, 286, 529
Urquhart J. S. et al., 2018, MNRAS, 473, 1059
Varricatt W. P., Davis C. J., Ramsay S., Todd S. P., 2010, MNRAS, 404, 661
Volvach L. N., Volvach A. E., Larionov M. G., MacLeod G. C., van den Heever S. P., Wolak P., Olech M., 2019, MNRAS, 482, L90
Vorobyov E. I., Elbakyan V. G., Liu H. B., Takami M., 2021, A&A, 647, A44
Zavagno A., Deharveng L., Nadeau D., Caplan J., 2002, A&A, 394, 225
Zhu Z., Hartmann L., Gammie C., McKinney J. C., 2009, ApJ, 701, 620

This paper has been typeset from a TEX/LATEX file prepared by the author.

Downloaded from https://academic.oup.com/mnras/article/522/2/2171/7120044 by University Library, University of Amsterdam user on 11 July 2024